Π
SPE36578

Horizontal Well Productivity and Risk Assessment

Kristian Brekke and Leslie G. Thompson, The University of Tulsa

This paper was prepared for presentation at the 1996 SPE Annual Technical Conference and Exhibition held in Denver, Colorado, USA, 6–9 October 1996.

Abstract

A fast and accurate method was developed for predicting long term horizontal well performance. Heterogeneous, anisotropic geology close to the wellbore were considered in addition to pressure loss through the completion. Speed and accuracy were achieved by replacing the well and reservoir simulation with a semi-analytical network approach, and by upscaling reservoir properties for radial flow. Comparison to fine grid reservoir simulations verify that both total well productivity and flux profile along the well are maintained for the simplified approach. Computational efficiency and comprehensive treatment of the horizontal well problem make the method suitable for complete incorporation of uncertainties connected to the completion, the near wellbore geology and formation damage. The procedure was applied to illustrate how uncertainties in geology and completion efficiency affect the distribution of total well productivity for finite and infinite conductivity horizontal wells of different lengths. The method proved to be very efficient for this type of study, and indicated positively skewed (log-normal like) productivity distributions for short wells, normal distributions for long wells and a tendency for negative skewness of the productivity distribution from pressure loss in the wellbore.

Introduction

Developments in drilling and completion technology have resulted in horizontal wells with longer wellbores, more complex geometry well paths and with sophisticated completion designs. These wells usually have a more complicated interaction with the reservoir than vertical wells. In addition, the parameters affecting the well performance also involve a higher level of uncertainty as compared to vertical wells.[1] Horizontal wells are affected by geological variations in the horizontal direction besides involving a larger variation in the outcome of the more complex drilling and completion operations. Thus, the application of long horizontal wells increases the potential both for success and failure. The potential for success can be enhanced by better understanding the total reservoir and wellbore interaction and flow behavior. Unexpected failures can be avoided by efficiently including all uncertainties in the predictions.

Throughout this study, the focus has been on the development and application of methodology for comprehensive prediction of production performance for horizontal wells. Besides providing accurate and CPU-time efficient calculation of the entire horizontal well flow problem, the methodology is developed for the purpose of incorporating the uncertainties connected to the near wellbore geology, formation damage and completion efficiency. In this study the theory used to describe the horizontal well flow problem is applied to three different regions as follows:

*1) **Flow through the near wellbore reservoir zone.*** Upscaling methods have been developed for radial flow in the formation close to the wellbore. The methods are based on a single phase, steady-state flow assumption. Fine grid simulations confirmed the development of a steady-state flow zone around the wellbore after a very short time. The upscaling methods incorporate the effects of convergent flow around the wellbore through heterogeneous and anisotropic formation. The theory and a computer program are developed for converting the description of a heterogeneous, anisotropic reservoir geology in Cartesian coordinates to an equivalent system in cylindrical coordinates for upscaling.

*2) **Flow in the Outer Reservoir.*** Two methods were considered for coupling well and near wellbore simulations to the response from the outer reservoir. The network model for the well and near wellbore reservoir can be coupled to a numerical reservoir simulator by an iterative coupling scheme. It is also shown how a semi-analytical pseudo steady-state reservoir response for non-uniform inflow and pressure profile along the well may be integrated with the well and near wellbore flow calculations through the network model. Productivities are derived by applying superposition in three dimensional space for the connection points between the near

wellbore reservoir zone and the outer reservoir.

*3) **Flow through the completion.*** For the wellbore, the applied pressure loss model accounts for the friction pressure loss and the additional pressure loss due to acceleration of the radial inflow to the wellbore.

The mass and momentum balance for the entire flow system are then solved by combining the flow regions in a nonlinear network solver developed in this study. Results from applying the developed methodology are verified by comparing to fine grid simulations using the Eclipse[2] numerical reservoir simulator. For single-phase flow through a highly heterogeneous near wellbore formation, both the total well productivity and the inflow profile along the well (obtained from the network model) correspond to the results from fine grid simulations. The effects of pressure loss along the completion on the well productivity and the magnitude of the acceleration's contribution to the pressure loss are illustrated.

A large number of heterogeneous realizations for the near wellbore reservoir zone were generated from variograms and an average value for the permeability by applying unconditional Sequential Gaussian Simulation.[3] These realizations formed the basis for the generation of well productivity distributions. Statistical results for the total well productivity are illustrated and discussed for cases of different well lengths and different levels of pressure loss along the wellbore.

Incorporating the Uncertainties Affecting Productivity

The comprehensive incorporation of the effects from uncertainties in different parts of a horizontal well system can theoretically be performed by applying traditional reservoir simulation techniques. However, to create a reliable probability distribution of well productivities may require several hundred simulation runs. The CPU time and the engineering labor combined with a large number of simulations are substantial. If productivity distributions are required for a variety of different completion and reservoir parameters such as correlation length, well length and well path, skin, completion diameter and roughness, the problem quickly becomes unmanageable with current technology. Thus, a flexible, sufficiently accurate and fast method for prediction of well performance is a critical element in a successful practical approach. Figure 1 illustrates the layout of the risk assessment procedure. A nonlinear network solver is indicated in the middle as being this critical element.

Average values and spatial correlation for the permeability may be present from information gained from wells in the same or similar reservoirs, seismic data or outcrops. A statistical method, in this case unconditional Sequential Gaussian Simulation, was used for generating multiple permeability fields for the near wellbore zone. If data from a pilot hole are available, conditional simulation may be applied to reduce uncertainty. The permeability fields are upscaled for a certain well trajectory and effective permeabilities are generated as input for the network solver.

Distributions for skin and completion roughness can be drawn from previously defined distributions. These distributions may be obtained empirically and are likely to be field specific. For this study, the distributions for skin and roughness were not made dependent upon other parameters. However, the skin distribution may be linked to the formation's exposure time to mud during drilling operation[4] and to local permeability at a given location along the wellbore.

The Steady-state Network Solver

The basic theory for linear network solvers has been well documented.[5] Linear network solvers are most thoroughly documented, but can be applied only for linear problems such as steady-state, single-phase flow of Newtonian fluids through porous media. For single-phase turbulent flow and multiphase flow along the well, and for multiphase flow through porous media, a nonlinear relationship exists between rate and pressure loss. One or all of these flow conditions are normally present in a horizontal well, and a nonlinear network solver[6,7,8] was, therefore, required. The solution to the problem has to be approximated by applying an iterative approach.

The network consists of nodes (connection points) and arcs (flow connections) as illustrated in Figure 2. The nodes may be configured as one of the following three types:

a) Unknown flowrate and pressure nodes (typically used for internal nodes)
b) Specified pressure, but unknown mass flowrate (typically used for boundary nodes)
c) Specified mass flowrate, but unknown pressure (typically used for boundary nodes)

For the resulting problem to be well posed, at least one terminal node should be a specified pressure node. The network flow problem is constructed from mass and momentum balances. As no accumulation of mass is allowed anywhere in the system, a mass balance, as given by Eq. 1, can be formulated for each node accounting for all mass entering or leaving the node through the connected arcs.

$$\sum_{i=1}^{n} \dot{m}_i = 0 \qquad (1)$$

In this equation, n is the number of arcs connected to the specific node.

Thus, internal nodes have a net mass flow of zero. Boundary, or terminal nodes may be assigned a net incoming or outgoing mass flowrate as shown in Eq. 2. Production from the node is assigned a negative mass flowrate and a positive mass flowrate denotes injection. In this case the pressure for the node is to be calculated.

$$\sum_{i=1}^{n} \dot{m}_i = \dot{m}_{in/out} \tag{2}$$

If the pressure rather than the mass flowrate, is being specified, the mass balance is omitted and an equation specifying the pressure is generated as given in Eq. 3.

$$p_j = p_{specified} \tag{3}$$

For each arc in the network a momentum balance can be defined which simply describes the pressure differential between the arc's upstream and its downstream connected node as a function of the mass flowrate. For nonlinear pressure loss versus mass flowrate relationships, the pressure loss through the arc for the new iteration level (k+1) can, by applying Newton's method, be expressed as:

$$\Delta p_{k+1} - \frac{\delta \Delta p_k}{\delta \dot{m}_k} \cdot \dot{m}_{k+1} = \Delta p_k - \dot{m}_k \cdot \frac{\delta \Delta p_k}{\delta \dot{m}_k} \tag{4}$$

The derivatives of pressure loss with respect to mass flowrate are found numerically for the arcs by perturbing the mass flowrate and performing two pressure loss calculations for each arc. Thus, the program requires routines to describe each arc's pressure loss for a given total mass flowrate. The combination of momentum and mass balances are finally arranged as a matrix problem and solved by using any standard sparse matrix solver.

Network Solver Applied in the Near Wellbore Zone

As the network model relies on the assumption of steady-state mass flow, its applicability for reservoir flow prediction is not obvious. However, if we assume that the part of the reservoir close to the wellbore attains steady-state flow after a short production time, the network simulator may be used to model the pressure and flow behavior in the near wellbore zone by ignoring short lived transient effects. It was found that for the purpose of long term production performance prediction transient effects in the reservoir close to the well could be ignored.[9]

Efficient use of the network solver in the near wellbore reservoir zone is dependent on some prior knowledge of the main flow direction with respect to the well. Far away from the well, where the pressure gradient is small, the direction of the flow may be strongly dependent on the geology and, thus, hard to predict. However, close to the well, where the pressure gradient in the direction of the well is significant, and the pressure gradient in any other direction is small, we found that radial flow perpendicular to the well is the dominant flow geometry. The radial flow assumption together with the steady-state flow assumption facilitate lumping of a large number of block permeabilities into one apparent permeability representing the flow and pressure behavior of the "real" fine grid heterogeneous case.

Figure 3 illustrates how the near wellbore zone can be implemented in the network solver. If a fine resolution heterogeneous description of reservoir properties is available (e.g., from applying geostatistical methods), this description is likely to be presented in a Cartesian grid. If we now imagine that we overlay the Cartesian grid with a cylindrical grid centered along the well axis, each cylindrical grid block will have a directional apparent permeability towards the well. The apparent directional permeability towards the well may be found by applying the upscaling methods for radial flow presented below. A single apparent permeability may be obtained for a full cylindrical block, or if a definition of inflow in the θ direction is required, the cylinder can be divided into "slices" with each having an upscaled permeability.

Blocks may also be averaged in the direction of the well without directly affecting the total well productivity significantly. However, a lumping of blocks in the well direction will smear out the inflow profile along the well and may, therefore, indirectly affect the total well productivity through the completion pressure loss calculations.

Permeability Upscaling. When upscaling a heterogeneous permeability formation close to the wellbore, we require that the flowrate-drawdown relationship for the well with the upscaled formation should resemble, as closely as possible, the flowrate-drawdown relationship for the well with the original, fine scaled near wellbore formation. For a horizontal well, the upscaling of permeabilities around the well also require some additional physics of the flow problem to be maintained:

1) As the pressure loss along the wellbore affects the well productivity, the inflow profile along the wellbore should be preserved through the upscaling process.

2) The pressure loss through an anisotropic near wellbore zone may be a strong function of θ. Thus, the method should allow generation of upscaled near wellbore segments for at least four discrete portions of the near wellbore cylinder (top, bottom, sides).

The upscaling method should handle variations in Cartesian block shape and resolution along the well. To effectively upscale for undulating wells, the upscaling procedure should handle any horizontal well location within a near wellbore zone element.

Two common approaches for upscaling small scale permeability variations into a larger scale apparent permeability are the "No Cross Flow" and the "Vertical Equilibrium" upscaling methods.[10,11] For linear flow upscaling, these methods have been combined into what is commonly called the "Incomplete Layer" method by performing an arithmetic averaging of the two.

The "No Cross Flow" and the "Vertical Equilibrium"

methods are applied here under the assumption that the flow in the upscaled zone is predominantly radial. Thus, the flow can be described with the steady-state equation for radial flow through porous media.

No-Cross Flow Upscaling. By assuming that the flow close to the wellbore is radial, the near wellbore zone of interest can be divided into separate flow sectors in the θ direction. The sectors are assumed to have no cross flow between them. Thus, the flowrate through any cross-section of a flow sector is independent of distance from the wellbore. This assumption motivates the application of Darcy's law for radial flow at different radial locations in a sector as illustrated in Figure 4. The sum of the pressure losses through the serially connected segments in a sector is the total pressure loss and the apparent permeability for each sector is the harmonic average permeability for all segments making up the sector, i.e.,

$$k_j = \frac{\ln(r_e / r_w)}{\sum_{i=1}^{n} \frac{1}{k_i} \cdot \ln(r_{i+1} / r_i)} . \qquad (5)$$

The other assumption applied in the No-Cross Flow upscaling method is a uniform pressure outer boundary for the area of investigation. The total pressure loss through all sectors is equal and the flowrates for all individual sectors add up to the total flowrate from the near wellbore zone of interest. This relationship is then used to determine an apparent permeability for either the entire circumference of the near wellbore zone or for a particular angular slice of the near wellbore zone, i.e., for all m sectors,

$$k_{app} = \frac{1}{m} \cdot \sum_{j=1}^{m} k_j . \qquad (6)$$

Combining Eqs. 5 and 6 provides the following final expression for the upscaled no cross flow permeability:

$$k_{app} = \frac{1}{m} \cdot \sum_{j=1}^{m} \frac{\ln(r_e / r_w)}{\sum_{i=1}^{n} \frac{1}{k_i} \cdot \ln(r_{i+1} / r_i)} \qquad (7)$$

Vertical Equilibrium (Full Cross Flow) Upscaling. The previously described No Cross Flow upscaling method focuses on the limiting case where flow only occurs in the radial direction and no flow occurs in the θ direction. The Vertical Equilibrium (Full Cross Flow) method considers the opposite extreme flow conditions and has already been applied to convergent flow around a wellbore.[12] It is assumed that the flux is evenly distributed around the perimeter of an annulus at any distance away from the well. Thus, the apparent permeability of an annular space in the permeability field can be found by applying a volume weighted arithmetic average of the Cartesian block permeabilities appearing in the annulus. An apparent permeability for either the whole or a particular angular slice of the near wellbore zone can then be derived as the harmonic average of the annulus permeabilities as given by

$$k_{app} = \frac{\ln(r_e / r_w)}{\sum_{j=1}^{m} \frac{1}{\frac{1}{n} \cdot \sum_{i=1}^{n} k_i} \cdot \ln(r_{j+1} / r_j)} . \qquad (8)$$

Transformation From Cartesian to Radial Grid System. As presented in the previous sections, the upscaling for radial flow in the near wellbore reservoir results in a straight forward and simple procedure as long as we operate on a cylindrical grid system. However, the permeability field we have to work with is more than likely to be presented in a Cartesian coordinate system. (The theoretical tools for reservoir characterization have been developed for a Cartesian system.) Thus, in order to perform upscaling for the convergent flow around the wellbore, it was necessary to develop theory for transformation[9] of the Cartesian based permeability field to a cylindrical coordinate system.

The basis for the transformation is to develop an apparent permeability for the cylindrical grid block which is made up of various heterogeneous Cartesian grid blocks. If we observe an arbitrary radial grid block, as given in Figure 5, it is apparent that the radial block can be sliced into a variety of smaller, odd shaped volumes by the Cartesian grid system. The geometric shapes and volumes of the Cartesian block contributions will depend on the rotation of the cylindrical grid block with respect to the Cartesian system and the relative resolution of the Cartesian to the radial grid. As the pressure gradient is large close to the wellbore, the radial grid block size is increased exponentially when moving away from the wellbore in the radial direction. Thus, even if the Cartesian grid block size is constant, the radial grid block size varies throughout the near wellbore zone and a wide range of relative block sizes are encountered.

The developed transformation attempts to calculate the volume of each Cartesian grid block contributing to the radial block in question and we apply these volumes as weighting factors in the averaging procedure. The contributing Cartesian blocks and the cylindrical blocks have the same length in the direction of the well. Thus, an area weighted average for the apparent radial block permeability given by the following expression applies:

$$k_r = (1 / A_r) \cdot (k_1 A_1 + k_2 A_2 + \ldots\ldots + k_n A_n) . \qquad (9)$$

Upscaling Anisotropic Formation. A critical factor determining the productivity of a horizontal well is the degree of anisotropy present. If the communication in the vertical direction is poor, the horizontal well productivity will suffer. The large scale anisotropy caused by layers of varying permeability is automatically taken into account in the upscaling process. However, anisotropy on a smaller scale has to be accounted for by considering the directional permeabilities throughout the near wellbore zone. Thus, a procedure for upscaling the near wellbore formation with different ratios of vertical to horizontal permeabilities[10] was implemented in the radial upscaling scheme.

The starting point for the anisotropic upscaling is the directional permeabilities for each Cartesian grid block. When applying the area based averaging procedure to determine the radial grid block permeabilities, a directional radial permeability can be calculated for the radial grid block from the x and y Cartesian system block permeabilities. The radial grid block orientation with respect to the wellbore is, unlike for the isotropic case, now of great importance as each Cartesian block contribution to the radial permeability is dependent on its direction from the wellbore. For the upscaling of radial flow around the wellbore, only the permeability in the vertical direction (z) and the horizontal direction perpendicular to the wellbore (x) is used. The horizontal permeability parallel to the well (y) is not applied in this process unless upscaling also is performed in the well direction. A schematic illustration of the anisotropic permeability problem is given in Figure 6.

Rotation of the coordinate system can now be applied and the directional, apparent permeability towards the wellbore can be found by combining the tensor elements according to the following equation[13]:

$$k_{r,app} = k_{xx} - \frac{k_{xz} \cdot k_{zx}}{k_{zz}} . \qquad (10)$$

The final relationship for the permeability in the direction perpendicular to the wellbore is given by

$$k_{r,app} = \frac{k_z \cdot k_x}{k_x - k_x \cdot \cos^2(\theta) + k_z \cdot \cos^2(\theta)} . \qquad (11)$$

The angle θ is measured from the Cartesian x axis to the line drawn from the grid block of interest towards the wellbore. The apparent radial permeability given in Eq. 11 is valid only for principle directions of anisotropy corresponding to the Cartesian x and z directions.

Implementing Outer Reservoir Response

The objective for applying the network simulator in the near wellbore zone is to reduce the computational problem by significantly reducing the involved number of grid blocks in a numerical simulation of the reservoir and well. However, the well and the near wellbore zone can not be considered an isolated flow problem uncoupled from the outer reservoir. The shape of the inflow profile has a profound impact on the productivity of the reservoir towards the boundary of the near wellbore zone. Thus, methodology for including the outer reservoir performance in the network model were investigated.

Coupling the Network Solver to a Numerical Reservoir Simulator. If the network solver is used to simulate only the wellbore and near wellbore formation, the transient response from the outer parts of the reservoir may be obtained by an iterative coupling to a numerical reservoir simulator. The feasibility of this procedure has already been proven[8] and the methodology described. Due to an underlying goal of simplicity and CPU efficiency, this option was not investigated further in this study.

Outer Reservoir Response From Superposition in Space. Since the scope of this work was to investigate long term productivities, we are interested in the pseudo-steady-state flow performance more than the early transient reservoir response. Several pseudo-steady-state relationships for horizontal wells are available in the literature. However, all these methods make the simplifying assumptions of either uniform flux or uniform pressure along the well. Models considering a random inflow profile or pressure profile along the well are not readily available. For the problem of modeling the pseudo-steady-state response from the reservoir outside a heterogeneous near wellbore zone, a non-uniform inflow and pressure profile model is required. The pressure loss inside the well will cause a non-uniform well pressure, and the pressure loss and rate through the near wellbore zone will vary with location along the well.

Similar to the near wellbore zone, the response from the remainder of the reservoir has to be divided into discrete sections along the well for inclusion in the network simulator. Unlike the near wellbore zone, the cross flow in the reservoir can not be neglected. The outer reservoir productivity for a connection point is highly dependent on the flowrate of the connection point in question. The connection productivity is also dependent on the production rates for the neighboring connection because the connection points are competing for drainage volume. The larger the rate for a connection point, the larger its drainage volume becomes and, as a result, productivity increases. Also, small production rates from neighboring connections favor a more pressure loss efficient shape of the drainage volume for the connection point in question. The productivity is, therefore, improved.

Thus, the interdependency of the connection points must be taken into account when calculating the productivities. Muskat developed steady-state theory[14] for multiple wells

inside a circular drainage area. He assumed two dimensional, steady-state flow. Muskat's theory is based on superposition in space. The method, originally presented for multi-well systems in two dimensions, was extended to three dimensions in this study, and, rather than considering multiple wells, superposition was performed for all the connection points between the reservoir and the near wellbore reservoir zone along a horizontal well. We assumed that the near wellbore zone elements could be regarded as small cavities in the shape of spheres and that the reservoir itself has the shape of a sphere. A schematic illustration of the configuration is given in Figure 7, where r_{wi} denotes the radius of each producing sphere, d_{ij} is the distance between two producing spheres and r_e is the radius of the reservoir sphere. For each connection point in three dimensional space, the pressure distribution can be represented by

$$p = C - \frac{q\mu}{4\pi k}\left(\frac{1}{r}\right). \quad (12)$$

The average pressure on the spherical reservoir boundary can be determined by adding the effects from each connection point using the average distance from the connection point to the boundary. The average boundary pressure is given by

$$p_e = c - \sum_{i=1}^{n} \frac{q_i\mu}{4\pi k}\left(\frac{1}{r_e}\right). \quad (13)$$

Here, c is a function of time which must be determined to ensure that material balance is preserved during pseudo steady state flow. This given value can be found either from performing an analytical material balance calculation or a reservoir simulation. For the more likely case where the reservoir takes a different shape than a sphere, the average radius from the well to the boundary is found as the radius of an equal volume sphere.

The pressure at any of the involved connection points between the reservoir and the near wellbore reservoir zone can now be determined by adding the contribution from all connection points. The connection pressures can be determined by the expression given in Eq. 14

$$p_{wfj} = c - \frac{q_j \cdot \mu_j}{4 \cdot \pi \cdot k}\left(\frac{1}{r_{wj}}\right) - \sum_{i=1, i\neq j}^{n} \frac{q_i \cdot \mu_i}{4 \cdot \pi \cdot k}\left(\frac{1}{d_{ij}}\right), \quad (14)$$

where c is the same as for Eq. 13.

The only remaining unknown parameter is the apparent wellbore radius for the sections of the near wellbore zone. This value can be found by matching the network model outer reservoir connection productivities to the productivities obtained from a reservoir simulation of the uniform wellbore pressure case. Thus, only one reservoir simulation is necessary to match the reservoir part of the network simulator and the network simulator will now work for any non-uniform inflow profile resulting from pressure loss along the wellbore or heterogeneous near wellbore geology.

If the network model is to be applied without the assistance of a reservoir simulator, the apparent radius of the spherical wellbore used in the superposition can be found by equating the surface areas of the spherical and the actual cylindrical near wellbore reservoir region.

It should be noted that the well is assumed to be located in the center of the reservoir. Thus, the inflow profile resulting from applying the method is not influenced by reservoir boundaries being closer to the ends of the well. The method also assumes an isotropic, homogeneous formation in the outer reservoir. An upscaling procedure based on spherical flow geometry is required for implementing the effects of anisotropy and heterogeneities in the superposition scheme. A pseudo-radial flow regime in the outer reservoir may be implemented by the use of image wells or by using other than the spherical flow equation.

Network Simulator Used to Model Flow Through the Completion

The flow inside a horizontal well differs from regular pipe flow because of the non-uniform flowrate along the well due to the influx from the reservoir. The fluids are continuously entering the wellbore from the upstream (toe) part of the well towards the downstream (heel) part of the well. An approximate solution can be obtained by dividing the wellbore into flow connections where the main flow connections represent the wellbore and the branched flow connections relate to the flow entering the wellbore through segments of the reservoir. The network solver can in this way be used to divide the wellbore into elements with increasing flowrates towards the heel part of the well. For single-phase, turbulent liquid flow through a wellbore arc, the pressure loss was modeled by using the equation for single phase flow frictional pressure gradient and a Moody type friction factor.

In addition to the frictional pressure gradient, an acceleration pressure loss is present along the wellbore. The flow configuration causing this pressure loss is illustrated in Figure 8. Both the fluid entering a wellbore arc from the upstream part of the wellbore (subscript u) and radially (subscript r) from the reservoir along the arc is being accelerated to their combined axial velocity (subscript d) at the downstream end of the arc. Several studies have been performed investigating this additional pressure loss, and Aasheim derived a relationship[15] for the acceleration pressure loss due to radial inflow given by

$$\Delta p_{Acc} = \frac{(\dot{m}_d v_d - \dot{m}_u v_u)}{A}. \quad (15)$$

This equation is based on a simple momentum balance

along the pipe past a perforation and assumes that the radial inflow is entering the completion with a zero velocity. Thus, no energy is assumed to be gained from the entrance velocity of the radial inflow. The model was in good agreement with experimental data[16] obtained from a large diameter test facility for axial flow with radial inflow.

Model Verification

Simulations were performed to verify each part of the network model separately. Initial simulations verified the use of upscaled permeabilities for the near wellbore zone. Simulations were also aimed at verifying the results from using superposition in space to obtain the outer reservoir response. Finally, comparative cases with anisotropic near wellbore zone and friction in the wellbore were run. Full detail of the verification runs can be found in Ref. 9.

Verification of the Permeability Upscaling Procedure. The integrity of the upscaling procedure was investigated by comparing the results from fine and upscaled grid reservoir simulations to the results from using the network model with upscaled near wellbore reservoir zone permeabilities. Two areas of particular interest were the conservation of total well productivity and inflow profile along the wellbore.

An Eclipse reservoir model with a fine grid and a heterogeneous permeability distribution in the near wellbore zone represented the 'true case'. Coarse and fine grid reservoir models with upscaled permeabilities around the wellbore and the network model with upscaled permeabilities were run under otherwise similar conditions.

The near wellbore zone had permeabilities ranging from 1.5md to 3000md, and a heterogeneity coefficient (standard deviation of permeability divided by mean of permeability) of 2.24 which can be expected for a well penetrating different facies. The near wellbore zone which originally consisted of 7260 grid blocks was reduced to 60 blocks through the upscaling procedure. Thus, the coarsening of the grid was considerable. However, the fine and coarse grid had equal resolution in the direction of the well. The base case used in this comparison had the following characteristics:

Reservoir Data:
Permeability outside near wellbore zone - 100 md
Porosity - 20%
Fine grid - 15x64x15 blocks (213m x 510m x 213m)
Coarse grid - 5x64x5 blocks (213m x 510m x 213m)

Near Wellbore Zone Data:
Fine grid - 11x60x11 blocks (11m x 310m x 11m)
Coarse grid - 1x60x11 blocks (11m x 310m x 11m)
Average permeability - 100md, Porosity - 20%
Variance (log-normal permeability distribution) - 50,000md^2
Spherical semi-variogram, Rx = 20m, Ry=20m, Rz=5m

Horizontal Well Data:
Length - 300m
Wellbore radius - 0.1m
Centrally located in the reservoir along the y direction
Number of connections between well and reservoir - 60

Fluids Data:
Single phase oil, μ_o = 1.82cP and ρ_o=811kg/m^3 - at reservoir conditions

The simulations were run with a uniform pressure along the well and with a constant oil flowrate of 100 Sm3/d. for a period of 11 days.

Fully Penetrating Horizontal Well. The upscaling procedure was developed to perform upscaling of permeabilities for radial flow. Thus, the method preserves the physics of the flow problem along the middle parts of the well. However, at the end points of the well, a spherical model would be required for an accurate upscaling. Thus, to eliminate potential errors stemming from end contribution effects, a fully penetrating horizontal well was first considered. A case where the original permeability field in Eclipse was replaced with the upscaled permeabilities while still using the fine grid was run to eliminate potential grid effects. The error in drawdown changed rapidly for both cases during the first fraction of a day, but stabilized after 0.5 days at a value of 4.0% for the vertical equilibrium case and at 0.05% for the no cross flow case.

The early errors are due to transient flow behavior in the near wellbore zone while steady-state flow was assumed in the upscaling process. The better performance for the no cross flow method indicates that the flow around the wellbore is radial. This was expected as the pressure gradient in this part of the reservoir is very large in the radial direction compared to in the θ direction.

However, for any CPU time saving benefit, the grid has to be coarsened according to the upscaling. Thus, the fine near wellbore grid of 7260 blocks is replaced with a grid consisting of 60 blocks, one block for each well connection. Figure 9 gives the percentage error in drawdown vs. time for this case. The same early transient behavior is present and the stabilized error in drawdown increased with 1.0% for both the incomplete layers method and the no cross flow method. Thus, a 1.0% error can be attributed to grid effects.

The results of the drawdown comparison and an inspection of the stream lines around the wellbore indicate that the no-cross flow method describes the flow behavior in the near wellbore reservoir zone more accurately than the vertical equilibrium method. Thus, only the no-cross flow method was further investigated.

As the goal was to replace the traditional numerical reservoir simulator with a network simulator, permeabilities from the no cross flow upscaling method were applied in the network simulator and used to calculate the pressure loss through the near wellbore zone. The radial flow Darcy equation was used as pressure loss model for the network flow connections.

At this point, we wanted to eliminate any discrepancy

between Eclipse and the network simulator in the handling of the outer part of the reservoir. Thus, a small shell (1.0m thick) of grid blocks was configured just outside the near wellbore zone to allow an estimation of the pressure at these locations. The network simulator was then run with these pressures as upstream boundary conditions rather than configuring additional flow connections describing the reservoir response. The pressures were obtained from the reservoir simulations at 11 days into production. The down stream boundary condition for the network simulator was a total production rate of 100Sm3/d.

The discrepancy in drawdown using the network simulator was 0.87%. Figure 10 shows a comparison of the inflow profile between the network simulator and the heterogeneous, fine scaled case. The oil inflow profile resulting from the network simulations generally agree very well with the inflow profile from the heterogeneous, fine grid simulations. As was observed in the previous comparison, the flowrate for connections with very large inflow is reduced by applying the network simulator.

It should be noticed that the pressure loss in the wellbore is not directly dependent on the inflow profile but rather upon the cumulative flow profile along the well. Thus, the effect from a small discrepancy in the inflow profile is weakened.

Partially Penetrating Horizontal Well. In a field application, the well is not likely to fully penetrate the reservoir in the horizontal direction. Thus, the previous comparison only verifies the upscaling methods to be used along the middle part of the well. As the developed upscaling procedure does not fully capture the physics of the flow problem at the ends of the well, some discrepancy in the inflow profile is expected between the 'true case' and the upscaled cases when the well is only partially penetrating the reservoir. However, if the well is sufficiently long, the produced error may not have significant impact on the total well productivity or pressure loss along the well. The reservoir was extended 100m beyond each end of the well.

The discrepancy in drawdown between the heterogeneous and upscaled case for partially penetrating well stabilized at 0.3% which is an improvement as compared to the results from the fully penetrating case. Thus, the error in upscaling end contribution effects counteracts some of the grid effects experienced from coarsening the grid.

Figure 11 illustrates the inflow profile along a partially penetrating well. A 10.0% error in inflow rate is now present for the end connections. In this case the end connections contribute 3.0% of the total production, and will for longer wells contribute even less. Thus, it can be concluded that the limitation in modeling end contribution effects in the near wellbore zone has negligible impact on the total productivity and the inflow profile for long horizontal wells.

Anisotropic Near Wellbore Zone. The validity of the method for implementing anisotropy in the permeability upscaling procedure was examined by comparing the results from a heterogeneous, fine grid reservoir model to the results from a coarse grid reservoir model with upscaled permeabilities for the near wellbore zone. Only the near wellbore zone had anisotropic permeabilities in both cases. For the fine grid case, each block in the heterogeneous near wellbore zone had vertical permeabilities of only 20.0% of the horizontal permeabilities.

For the upscaled, coarse grid case an apparent radial permeability was applied for each block. The apparent permeability was provided for use both as x and z permeabilities in the reservoir simulator. Thus, this permeability could as well have been provided to the network model for approximately the same results. The percentage error in drawdown (or total productivity) stabilizes at -0.3% at 0.5 days. Thus, the effect of anisotropy was being well captured by the proposed procedure. Again, the inflow profiles were compared and found to agree satisfactorily. No additional error due to the implementation of anisotropy was detected.

Verification of Pseudo Steady-State Reservoir Response from Superposition in Space. The superposition scheme for implementation of the outer reservoir response in the network simulator was tested versus the performance of Eclipse using a model with a more refined outer reservoir grid than used in previous cases. The 100m extension of the reservoir in all directions from the well was in this case divided into 25m blocks. Since it was already verified that the upscaled representation of the near wellbore zone gave satisfactory results, the coarse near wellbore grid reservoir model was used as the 'true case' in the comparison.

A homogeneous case with a permeability of 100md, with uniform pressure along the wellbore and with a constant production rate of 100Sm3/d was simulated with Eclipse. Both the connection pressures and flowrates along the interface between the near wellbore zone and the outer reservoir were recorded. Using the grid block pressures along the boundary of the reservoir, an average reservoir boundary pressure was calculated. From this information, the productivity of the outer reservoir could be calculated for all connections along the well.

The same case was configured in the network model with a total of 180 flow connections for the well, near wellbore zone and the outer reservoir. The average reservoir pressure and the well pressure recorded from the reservoir simulation were applied as boundary conditions. The apparent radii of the spherical wellbores used for the outer reservoir flow connections were adjusted until a total flowrate of 100Sm3/d was obtained. An apparent wellbore radius of 7.0m matched these results. Figure 12 shows a comparison of the productivity profiles at 111 days resulting from both Eclipse

and the network solver. The productivity profiles correspond satisfactorily and show that the applied superposition scheme captures the physics of the outer reservoir flow for the homogeneous, uniform wellbore pressure case.

The case with a heterogeneous near wellbore zone was then tested to see whether large differences in connection flowrates would compromise the accuracy of the superposition scheme. The network model was used with the apparent wellbore radii already found from the homogeneous case and the reservoir simulator was again run with a constant production rate of 100Sm3/d. The network model was now equipped with the upscaled near wellbore zone permeabilities and had the average reservoir boundary pressure and the well pressure recorded from the reservoir simulation at 111 days as boundary conditions. For this case, the total production rate from using the network simulator was 99.7Sm3/d which is within 0.3% of the flowrate calculated from Eclipse. Figure 13 shows a comparison of the inflow profile along the well for both simulators. The inflow profiles are in good agreement and show that the superposition procedure can be applied for a non-uniform inflow and pressure profile along the near wellbore zone. Thus, various cases may now be run with the network model for different wellbore and near wellbore configurations.

Finite Conductivity Wellbore Case. As an illustration of the methodology's capability, a case with an internal diameter of the completion of 1.0in. internal diameter (ID) was run with the network simulator and compared to the no friction case. The small ID was chosen to emphasize the effects of pressure loss and is not necessarily recommended practice for a field application. Figure 14 compares both the pressures along the wellbore and along the near wellbore zone for the two cases. For the friction case, an exponential drop in wellbore pressure is seen towards the down stream parts of the well.

The acceleration contribution to the pressure gradient in the wellbore is plotted versus location in Figure 15. For most parts of the well, the contribution from acceleration is small, and is proportional to the amount of inflow relative to the axial flowrate. The highest percentage contribution from acceleration (10%) is seen at the upstream (block #60) part of the well, where the frictional pressure loss is low. However, the absolute magnitude of the acceleration pressure loss increases towards the downstream (block #1) part of the well where the total pressure gradient is large.

The influence on the inflow profile from pressure loss along the well is illustrated in Figure 16. Starting from the toe and moving towards the heel, the inflow per connection is considerably reduced along the first 70% of the well. The lost production is made up for by additional production along the last 30% of the well. For the friction case, the drawdown at the heel of the well is increased by 350%. Thus, the loss of total well productivity due to friction along the wellbore was, for this case, 70%.

Example Application, Uncertainties in Total Well Productivity

To illustrate the potential benefits from applying the developed approach, the network model was used in a statistical study to generate probability distributions for the total well productivity of a horizontal well. The objective was to detect how parameters such as well length and friction through the completion would influence the probability distribution for well productivity.

Unconditional Sequential Gaussian Simulation was used to generate 300 isotropic, heterogeneous near wellbore permeability fields that satisfied a log-normal permeability distribution with a mean of 100md and a variance of 50,000 md^2. The geometric layout of the reservoir was kept similar to the above described verification model for a partially penetrating horizontal well. However, horizontal and vertical correlation lengths (variogram range) of 150m and 1.5m, respectively, were selected as a base case for more field like conditions.

Each of the 300 near wellbore realizations were upscaled from 7260 permeabilities to 60 apparent permeabilities for use in the network simulator. The outer reservoir response was implemented in the network simulator as for the above explained verification runs.

The network model was run with and without friction through the completion for all near wellbore realizations. Well length was varied in steps between 50m and 300m.

Infinite Conductivity Cases. A distribution consisting of 300 total well productivities was obtained for each well length. Figure 17 gives the average well productivity, the most likely well productivity (mode) if only one well is being considered, and the boundaries where 20% and 80% of the productivities fall below the indicated value. All productivities are given as productivity per unit well length.

For very small well lengths, the average of the productivity per unit well length is high due to an efficient spherical flow geometry in the reservoir. However, if one was to drill only one well, the most likely outcome of this well would be equivalent to the mode for the distribution. For well lengths shorter than the correlation length (range of the variogram), the mode of the distribution is considerably lower than the average. For a well length of 25m, the most likely outcome of a one well operation would be among the 20% cases with the lowest productivity. This indicates that the distribution is skewed to the right (log-normal like shape).

As pointed out in the literature[1], a log-normal distribution of productivities may be expected due to log-normally distributed permeabilities. This is the case for horizontal wells with small effective well lengths. Since productivity is strongly dependent on the near wellbore zone permeabilities, the productivity distribution will resemble the permeability distribution.

However, for well lengths approaching or exceeding the

horizontal correlation length (variogram range), a normal distribution is expected. For a long well with infinite conductivity wellbore, we assume that the well productivity is an approximate linear function of the average of the near wellbore zone permeabilities and that a sufficiently long well contacts an adequately large sample of the permeability distribution. The linearity of the relationship between well productivity and the average near wellbore zone permeability depends on the relative magnitude of the pressure loss through the near well bore zone when compared to the total pressure loss through the reservoir. If this relative magnitude is large, we are indirectly sampling a linear function of the average of the permeability field and the outcome should according to the Central Limit Theorem[17] be a normal distribution. The Central Limit Theorem simply states that the a sampled average of any distribution forms a normal distribution. From Figure 17 it can be observed that the average and the mode of well productivity approach the same value for well lengths greater than the horizontal range of the variogram. This indicates a normal distribution. The same argument can be made by inspecting the shape of the productivity distributions for well lengths of 25m and 300m given in Figures 18 and 19, respectively.

Thus, if a well effectively contacts the formation through at least one correlation length (range of the variogram), one may expect the productivities to be normally distributed. This assumes that the entire length of the wellbore is open for inflow, which may not be the case due to formation damage, poor cleanup or too sparsely perforated cemented liners.

By inspecting the 20% and 80% limits for productivity in Figure 17, it can be seen that the uncertainty in well productivity decreases with increasing well length. Again assuming that the productivity is a sufficiently strong function of well block permeabilities alone, the Central Limit Theorem suggests that the variance of productivity per unit well length for undamaged wells with no friction in the wellbore is proportional to the inverse of the well's length. To support this theory, the variance of productivity per unit well length multiplied with the well length is plotted versus well length in Figure 20. It can be noted that this parameter becomes approximately constant for well lengths greater than the horizontal correlation length (variogram range).

Finite Conductivity Cases. For the finite conductivity wellbore cases, an internal completion diameter of 1.5in. was selected. The roughness of the completion may for a real case vary dependent on several factors such the quality of completion manufacturing, installation and clean-up. Thus, to include this uncertainty, the absolute roughness was for each liner segment picked randomly from a uniform distribution between 0.1mm and 20mm.

Figure 21 gives for finite conductivity cases the same information as given in figure 17 for infinite conductivity cases; the average well productivity, the mode and the 20% and 80% limits. For very short well lengths, the values are comparable to the no-friction cases. However, as well length increases, the mean and the 80% limit decline rapidly due to the effects of friction in the well. The 20% limit is not as strongly affected by friction for short and medium well lengths. Figure 22 compares the average of total productivity for friction and no friction cases. It is apparent that extending the well length beyond 300m has little or no effect on the total productivity when friction is included in the calculations. For the no friction case, a proportional increase in productivity is seen for increasing well lengths. It should also be noticed that the uncertainty in productivity is reduced considerably by the introduction of friction in the well.

Thus, in addition to shifting the probability distribution, friction also has an effect on the shape of the distribution. For well lengths up to a certain limit, friction has a considerably stronger damaging effect on the productivity for high productivity than low productivity cases. Thus, friction skews the distribution towards smaller productivities. This can be seen from the behavior of the mode, which increases rapidly and for medium well lengths, is greater than the average productivity. In Figure 23 the finite conductivity productivity is plotted as a fraction of infinite conductivity productivity and versus infinite conductivity productivity. All cases are for a well length of 50m. Obviously, the damaging effect from friction is a strong and almost linear function of well productivity.

However, if well length is further increased, the damaging effect from friction tends to discriminate less among the cases. Thus, a more constant shift of the distribution is seen. This is supported by Figure 21 where it can be noted that the mode and the average approach the same value again for long wells. For 300m long wells, the reduction in productivity due to friction is given vs. productivity in Figure 24. A more constant reduction of productivity can be seen for a wide range of high productivities.

At first glance, this might seem unreasonable since the pressure loss as a rule has a more unfavorable effect on the productivity of high productivity wells than low productivity wells. However, the effect seen is reasonable since the magnitude of the frictional losses depends on the average flow length for the fluid though the completion. For low productivity cases with a fairly uniform influx, this average length approaches 1/2 of the total well length and the friction pressure loss is large. High productivity cases have most of the fluids entering into the wellbore at the downstream parts of the well which results in a considerably smaller average flow length and smaller frictional pressure loss. Thus, there appears to be a limit to the productivity reduction due to friction pressure loss in the wellbore. This is an increasingly dominant effect as well length is increased.

Lower Productivity		***Higher Productivity***
Smaller effect from larger dp_{fr}	$\approx$	Larger effect from smaller dp_{fr}.

Efficiency of Network Approach. The CPU time combined with the upscaling procedure was 10 hours on a Pentium PC, but may be reduced considerably by taking advantage of geometric repetitiveness along the near wellbore zone and between the cases and by focusing on the no-cross flow upscaling procedure alone. A total number of 4800 simulations were automatically performed with the network simulator for this study. These simulations took 1/2 hour to run on a Pentium PC, while fine grid simulations using Eclipse on a HP 700 would have taken on the order of 400 hours to run.

Conclusions

1. A network simulator capable of solving nonlinear networks has been developed and successfully applied for comprehensive flow prediction of horizontal wells producing single-phase fluids. The simulator is capable of combining the effects resulting from non uniform wellbore pressure and from heterogeneous and anisotropic permeabilities near the wellbore. The network model predicts well productivity within an accuracy of 1% when compared to fine grid reservoir simulations.

2. A method based on superposition in space has been developed and implemented in the network model to include pseudo steady-state reservoir response for an arbitrary pressure and inflow profile along the well. Thus, a time dependent well performance can be obtained without performing transient reservoir simulations.

3. An upscaling procedure for single-phase radial flow in heterogeneous, anisotropic near wellbore formation has been developed, tested and successfully applied to drastically reduce the grid resolution needed to accomplish accurate flow predictions for horizontal wells.

4. Upscaling by applying the no cross flow assumption around the wellbore appears to be the superior method for the cases investigated in this study.

5. A procedure for converting block permeabilities from a Cartesian to a cylindrical coordinate system was developed, implemented and applied to facilitate radial flow upscaling.

6. An existing model for acceleration pressure loss in horizontal wells producing single-phase fluids was verified through flow experiments and implemented in the network approach.

7. By using the proposed approach to perform an example statistical study of the total well productivity, the required CPU time was reduced by a factor of 40 (with potential for improvement) as compared to using a numerical reservoir simulator.

8. Statistical analysis of the well productivity due to variations in near wellbore geology indicated a log-normal (skewed to the right) distribution of productivities for well lengths shorter than the horizontal correlation length (range).

9. As the well length approach or exceeds the horizontal correlation length, a normally distributed probability distribution is obtained for the horizontal well's total productivity.

10. Friction in the wellbore generally skews the productivity distribution to the left.

11. There appears to be a limit in productivity for which the reduction in productivity due to friction in the wellbore becomes constant. This is increasingly dominant for long wells.

12. For longer wells than the horizontal correlation length, the variance of productivity per unit well length is approximately proportional to the inverse of the well's length.

Nomenclature

A	= area (m^2)
e_D	= relative roughness
f	= friction factor (Moody)
h	= length of reservoir section (m)
l	= length (m)
$\dot{m}$	= mass flowrate (kg/s)
N_{Re}	= Reynolds number
p	= pressure (kPasc.)
q	= flowrate (m^3/d)
r	= radius
v	= velocity (m/s)
ρ	= density (kg/m^3)
μ	= viscosity (cp)
θ	= angle from horizontal

Subscripts

app	= apparent
e	= relates to outer boundary
d	= down-stream
k	= iteration counter
tot	= total
u	= up-stream
w	= wellbore

Acknowledgments

The authors would like to thank the member companies of University of Tulsa Petroleum Reservoir Exploitation Projects

for their support. We also extend our appreciation to the Norwegian Research Council for their financial support throughout this project. We would also like to thank Thormod Johansen, Albert Reynolds and Ekrem Kasap for useful discussions, comments and ideas.

References

1. Beliveau D.: "Heterogeneity, Geostatistics, Horizontal Wells, and Black Jack Poker," *SPE Journal of Petroleum Technology*, December 1995, pp 1068-1074.
2. Eclipse 100, Release 94A, Reference Manual, Intera Information Technologies Limited, England
3. Deutsch, C. V. and Journel, A. G.: "GSLIB - Geostatistical Software Library and Users Guide," New York / Oxford, Oxford University Press, 1992.
4. Engler T. W., Osisanya S. and Tiab D.: "Measuring Skin While Drilling", paper SPE 29526 presented at the Production Operations Symposium, Oklahoma, 1995.
5. Dolan A. and Aldous J.: "Networks and Algorithms," John Wiley and Sons, Chichester (1981).
6. Asbjornsen O. A.: "Algoritms and Programs for the Solution of General Fluid Flow Networks," Internal Report, Norsk Hydro, 1990.
7. Brekke K. and S. C. Lien: "New, Simple Completion Methods for Horizontal Wells Improve Production Performance in High Permeability Thin Oil Zones," *SPE Drilling and Completion*, September 1994, pp 205-209.
8. Brekke K., T. E. Johansen and R. Olufsen: "A New Modular Approach to Comprehensive Simulation of Horizontal Wells," paper SPE 26518 presented at the 68th. SPE Annual Technical Conference and Exhibition, Houston, 1994.
9. Brekke, K.: "Productivity and Risk Assesment for Horizontal Wells," Ph. D. dissertation, University of Tulsa, OK (1996).
10. Kasap, E., Class Notes: "Upscaling of Reservoir Heterogeneities," The University of Tulsa, OK (1995).
11. Kasap, E. *et al*: " Calculating the Effective Permeability Tensor of a Grid Block," *SPEFE*, June 1990.
12. Sagar, R.: "Reservoir Description by Integration of Well Test Data and Spatial Statistics," Ph. D. dissertation, University of Tulsa, OK (1993).
13. Aasum, Y *et al*: "Analytical Up-scaling of Small Scale Permeability Using a Full Tensor," *Petroleum Geoscience*, (Vol 1, no. 4, 1995), European Association of Petroleum Geoscientists.
14. Muskat, *Flow of Homogeneous Fluids Through Porous Media*, McGaw Hill, 1937.
15. Aasheim, H.: "A Flow Resistance Correlation for Completed Wellbore," *Journal of Petroleum Science and Engineering*, (vol. 8), 1992, pp 97-104.
16. Brekke K, A. Valle and Utvik, O. H.: "Two Phase Flow in Horizontal Wells," PROFIT, a project directed by "det Norske Petroleumsdirektorat" , 1994.
17. Hogg, R. V. and J. Ledolter, *Applied Statistics for Engineers and Scientists*, Macmillan Publishing Co., USA, 1992.

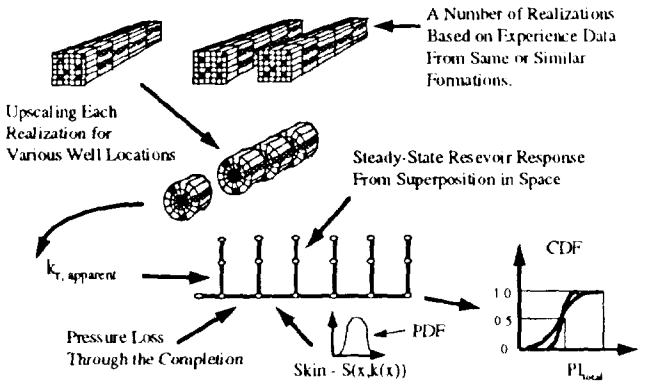

Fig. 1 - Uncertainty Assessment Procedure - Overview

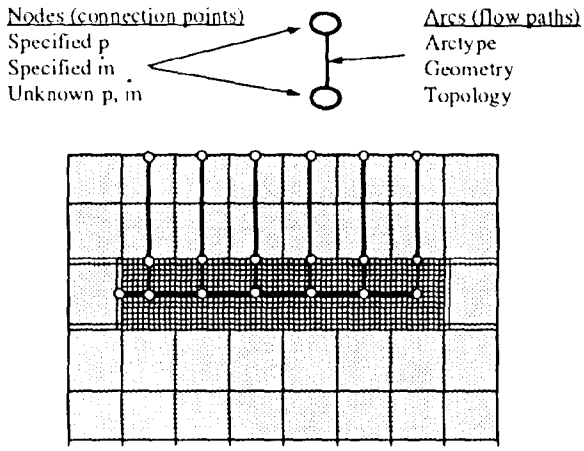

Fig. 2 - Steady State Network Solver - Schematics

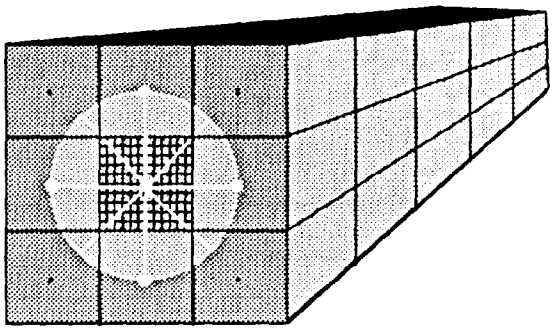

Fig. 3 - Network Solver Applied in the Near Wellbore Reservoir Zone - Schematics

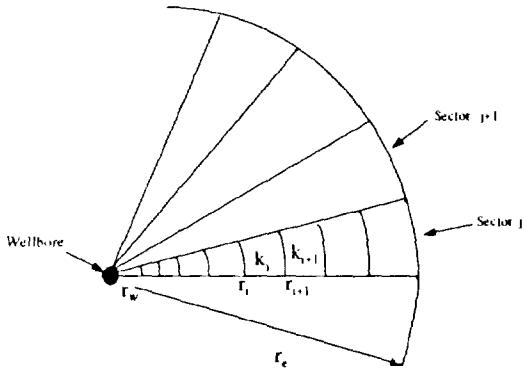

Fig. 4 - No Cross Flow Upscaling For Radial Flow - Schematics

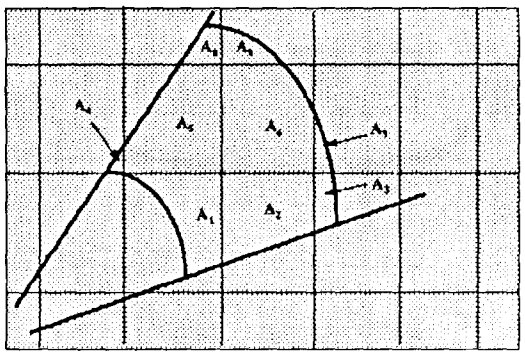

Fig. 5 - Volumetric Averaging of Radial Block Permeability - Schematics

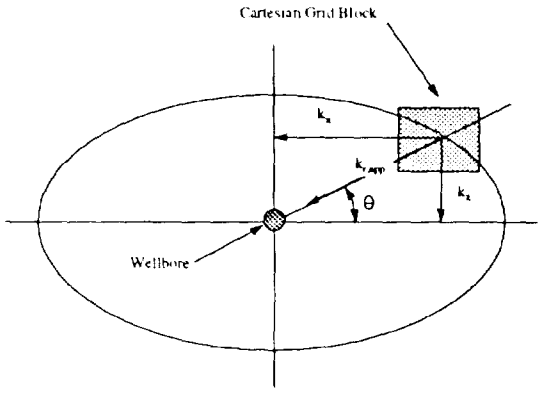

Fig. 6 - Apparent Anisotropic, Radial Permeability - Schematics

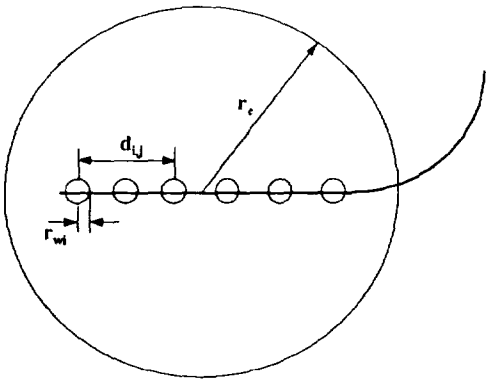

Fig. 7 - Outer Reservoir Response From Superposition in 3D Space - Schematics

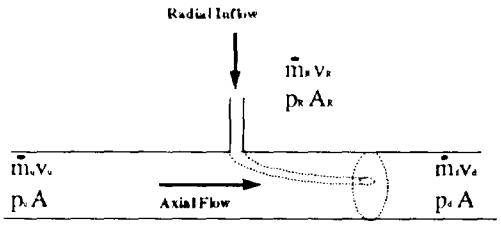

Fig. 8: Acceleration Pressure Loss Through Completion due to Radial Inflow - Schematics

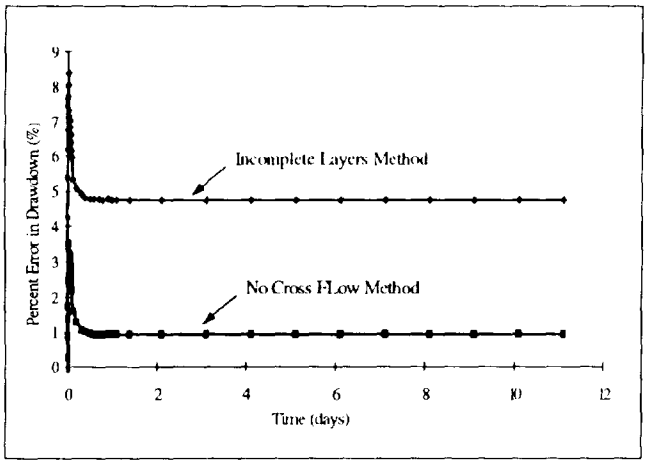

Fig. 9 - Error in Drawdown vs. Time - Eclipse with Coarse Grid and Upscaled Permeabilities versus Fine Grid and Heterogneous Permeabilities - Fully Penetrating Horizontal Well

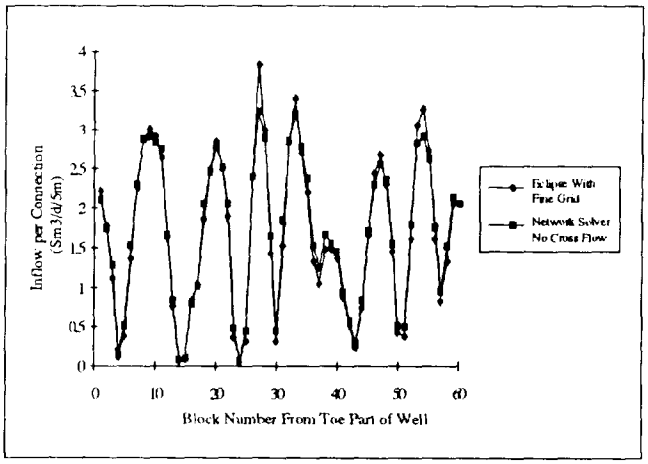

Fig. 10 - Oil Inflow vs. Location Along Well, Comparison - Fully Penetrating Horizontal Well, Eclipse With Fine Resolution Grid and Network Solver with No Cross Flow Method Used for Upscaling

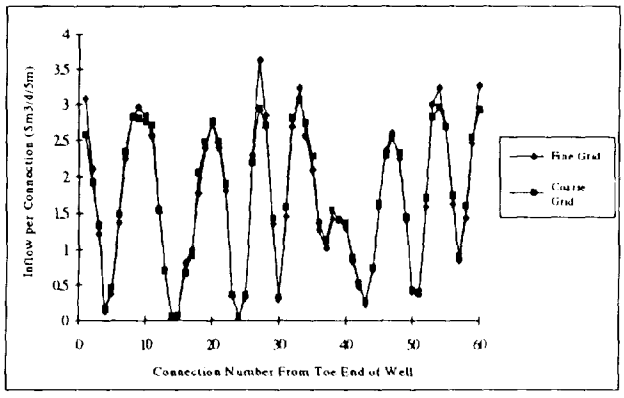

Fig. 11 - Oil Inflow vs. Location, Eclipse with Coarse Grid and Upscaled Permeabilities versus Fine Grid and Heterogneous Permeabilities - Fully Penetrating Horizontal Well

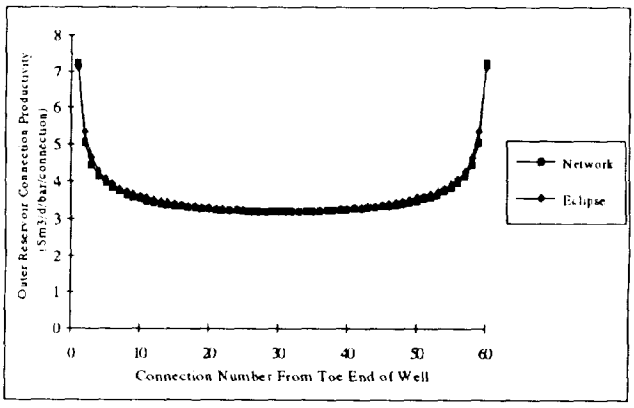

Fig. 12 - Outer reservoir Productivity Profile Comparison - Eclipse and Network Solver - 111 Days Into Production

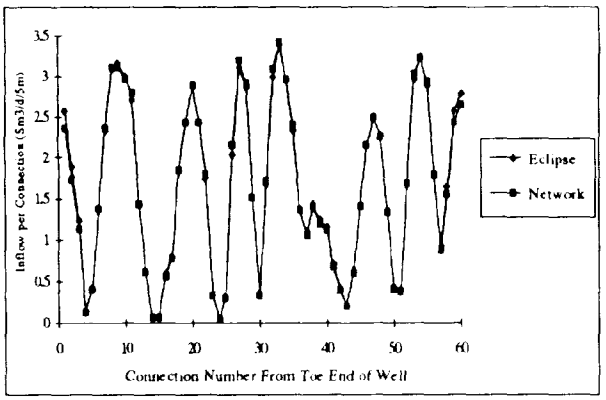

Fig. 13 - Oil Inflow vs. Location Along Well, Comparison, Partially Penetrating Horizontal Well - Eclipse vs. Network Simulator With Superposition In Space used for Outer Reservoir

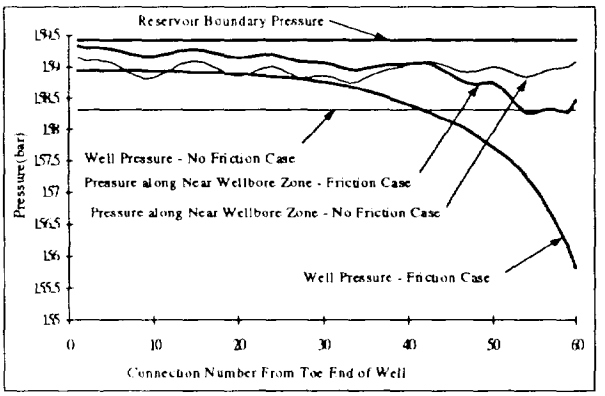

Fig. 14 - Pressure Profile Comparison - Partially Penetrating Horizontal Well - Friction Less Wellbore vs. 1.0" ID Wellbore

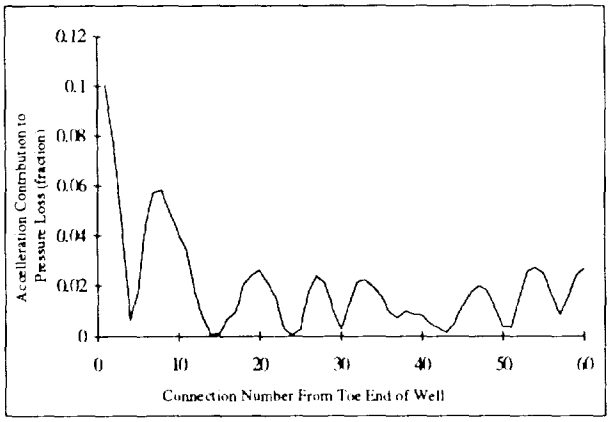

Fig. 15 - Accelerational Contribution to Wellbore Pressure Gradient vs. Location Along the Well

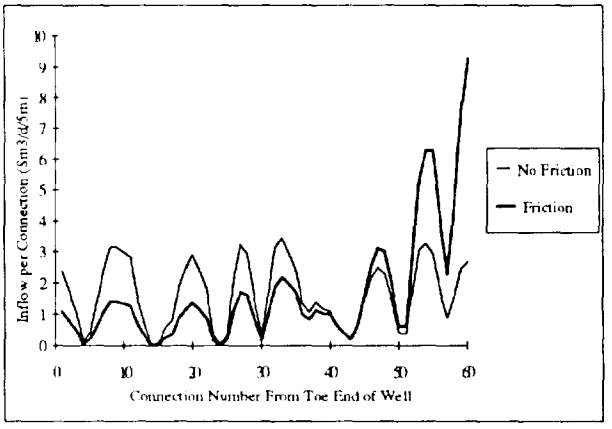

Fig. 16 - Friction vs. No Friction Inflow Profile Comparison - Partially Penetrating Horizontal Well

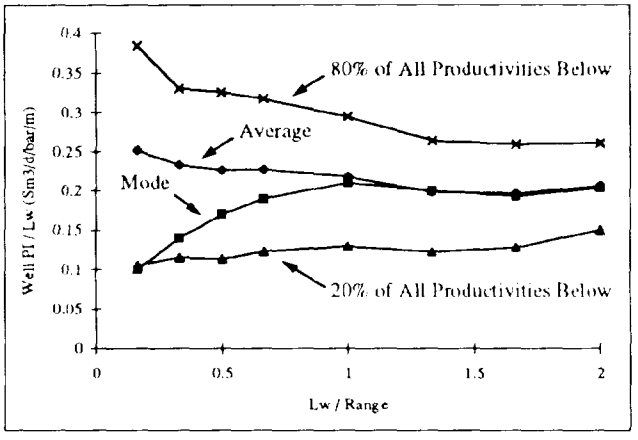

Fig. 17 - Infinite Conductivity Wellbore - Average, Most Likely, 20% Limit and 80% Limit of Total Productivity / Well Length vs. Well length / Range

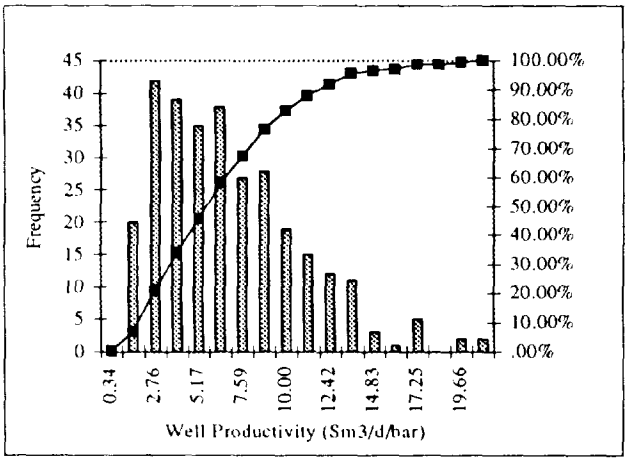

Fig. 18 - Probability Distribution for Well Productivity at 111 days into Production, Well Length = 25 m, Infinite Conductivity Wellbore

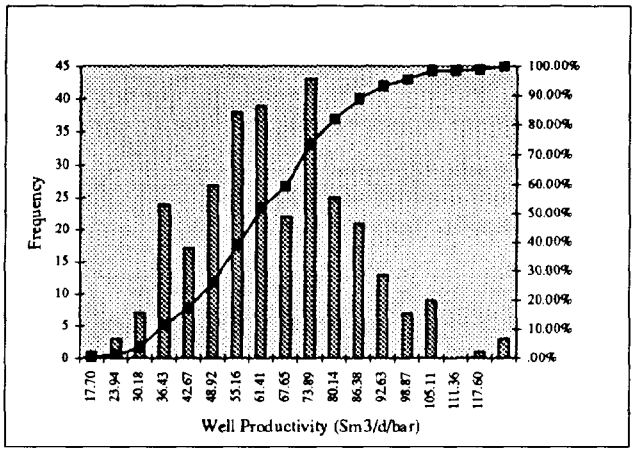

Fig. 19 - Probability Distribution for Well Productivity at 111 days into Production, Well Length = 300m, Infinite Conductivity Wellbore

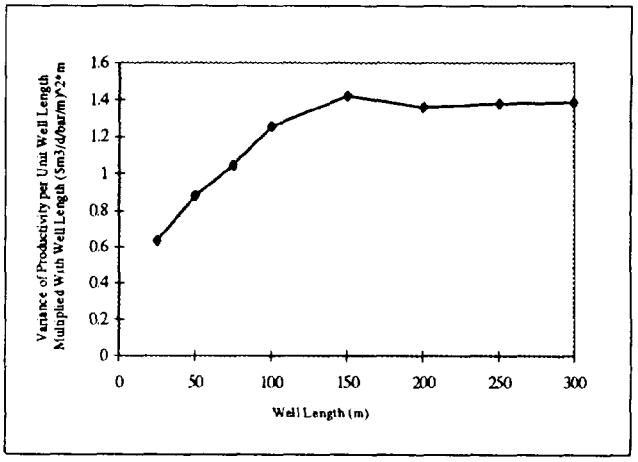

Fig. 20 - Infinite Conductivity Wellbore - Variance of Productivity per Unit Well Length times Well Length vs. Well Length

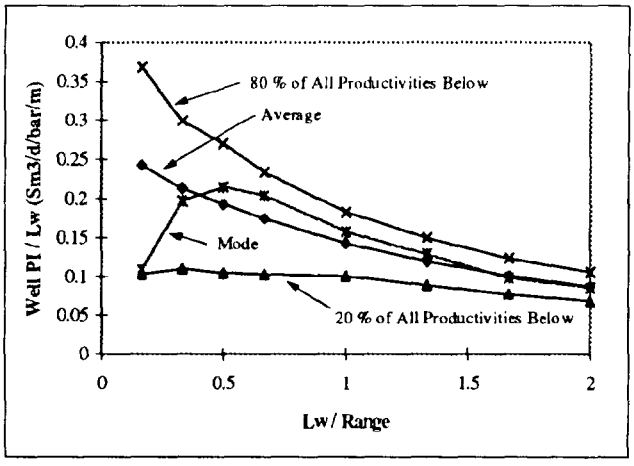

Fig. 21 - Finite Conductivity Wellbore - Average, Most Likely, 20% Limit and 80% Limit of Total Productivity / Well Length vs. Well length / Range.

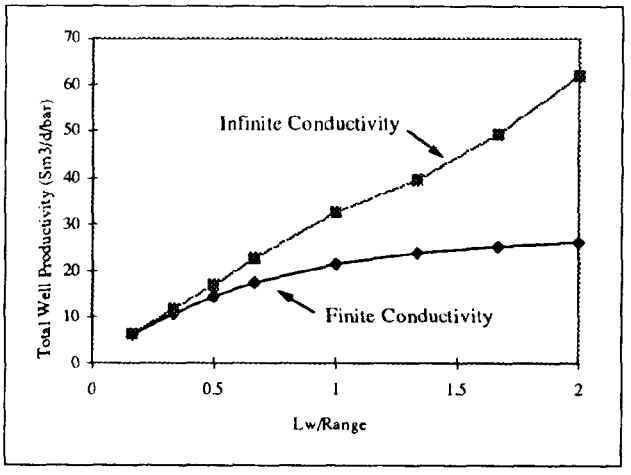

Fig. 22 - Comparison of Average Total Well Productivity - Infinite and Finite Conductivity Wellbore

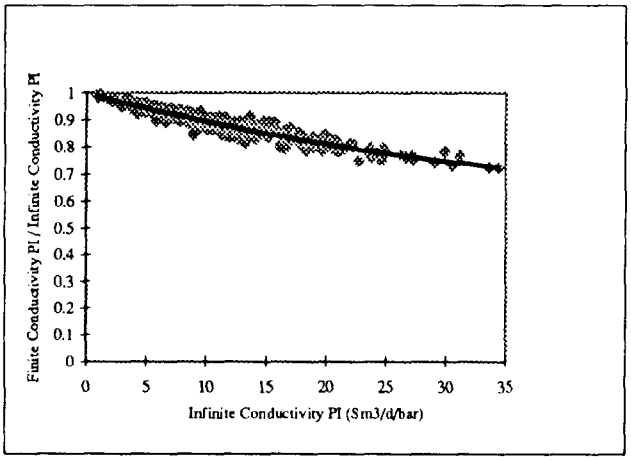

Fig. 23 - Finite Conductivity PI as Fraction of Infinite Conductivity PI vs. Infinite Conductivity PI - Well Length = 50m

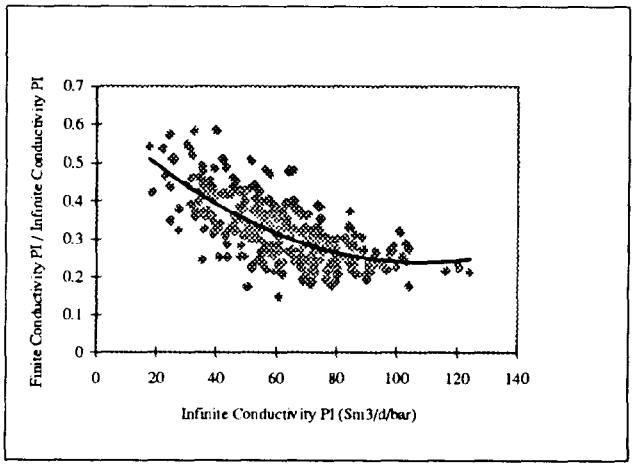

Fig. 24 - Finite Conductivity PI as Fraction of Infinite Conductivity PI vs. Infinite Conductivity PI - Well Length = 300m